

# Simulation of the Flow past a Circular Cylinder Using an Unsteady Panel Method

**Ramos García, Néstor; Sarlak Chivaee, Hamid; Andersen, SørenJuhl; Sørensen,Jens Nørkær**

*Published in:*
Applied Mathematical Modelling

*Link to article, DOI:*
10.1016/j.apm.2016.12.001

*Publication date:*
2017

*Document Version*
Peer reviewed version

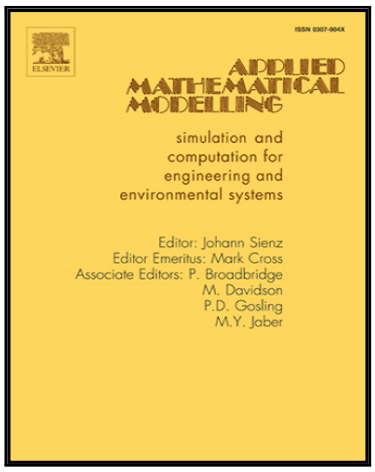


# Simulation of the Flow past a Circular Cylinder Using an Unsteady Panel Method

N. Ramos-Garcõa, H. Sarlak, S.J. Andersen, J.N. S¿rensen

PII: S0307-904X(16)30642-4
DOI: 10.1016/j.apm.2016.12.001
Reference: APM 11463

To appear in: *Applied Mathematical Modelling*

Received date: 11 February 2016
Revised date: 4 November 2016
Accepted date: 7 December 2016

Please cite this article as: N. Ramos-Garcõa, H. Sarlak, S.J. Andersen, J.N. S¿rensen, Simulation of the Flow past a Circular Cylinder Using an Unsteady Panel Method, *Applied Mathematical Modelling* (2016), doi: 10.1016/j.apm.2016.12.001

## Highlights

- The in-house UnSteady Double Wake Model USDWM is presented in the manuscript.
- Sub-, super-, and trans-critical cylinder flows have been successfully simulated.
- The results show a good comparison between USDWM, URANS, and experiments.
- USDWM is capable of capturing the dynamics of the flow.
- USDWM is capable of capturing changes in St, Cd and Cp for the three regimes.

# Simulation of the Flow past a Circular Cylinder Using an Unsteady Panel Method

N. Ramos-Garc´ıa[a,*], H. Sarlak[b], S.J. Andersen[a], J.N. Sørensen[a]

[a]*Department of Wind Energy, Fluid Mechanics Section, Building 403, Technical University of Denmark, DK-2800 Lyngby Denmark*

[b]*Centre for Flow Measurement and Fluid Mechanics, Faculty of Engineering and Computing, Coventry University, Coventry CV1 5FB, United Kingdom*

## Abstract

In the present work, an in-house UnSteady Double Wake Model (USDWM) is developed for simulating general flow problems behind bodies. The model is presented and used to simulate flows past a circular cylinder at subcritical, supercritical, and transcritical flows. The flow model is a two-dimensional panel method which uses the unsteady double wake technique to model flow separation and its dynamics. In the present work the separation location is obtained from experimental data and fixed in time. The highly unsteady flow field behind the cylinder is analyzed in detail. The results are compared with experiments and Unsteady Reynolds-Averaged Navier Stokes (URANS) simulations and show good agreement in terms of the vortex shedding characteristics, drag, and pressure coefficients for the different flow regimes.

*Keywords:*

circular cylinder, unsteady flow, panel method, vortex method, URANS

*Corresponding author

*Email address:* nerga@dtu.dk (N. Ramos-Garc´ıa)

## 1. Introduction

Wind turbines have grown tremendously in size in the past decades[1], and turbines are now approaching 10MW and future generations of even larger turbines. Larger turbines provide new challenges for scientists and engineers in the wind energy community. One of the main challenges is structural as the new and larger designs demand longer and more slender blade designs. However, close to the root the long blades require thick airfoils, which offers new challenges for the sector as traditional airfoils development have been based on relative thin airfoils for *e.g.* planes. Designing new and innovative generations of thick airfoils has become one of the main obstacles that aerodynamicists face nowadays. Flow separation remains one of the main difficulties in the field of fluid mechanics, and it becomes particularly critical in the case of thick airfoil profiles.

It is well-known that it is a hard task to correctly predict the behaviour of the complex vortex shedding behind thick bodies, even for highly sophisticated Navier-Stokes solvers with advanced turbulence models. Furthermore, such solvers require fine meshes and a high amount of computational power, which are often impractical during design iterations.

Therefore, panel or vortex methods present viable alternatives to the Eulerian Navier-Stokes solvers. These methods follow a grid-free Lagrangian approach with vortex shedding and tracking, and have been employed to capture the overall physics of separated flows over airfoils in the last four decades. Maskew and Dvorak [1] developed a simplified model based on an inviscid flow solver, which could accurately simulate steady flows around airfoils at high angles of attack. Following this idea, Ramos-Garc´ıa[2] developed a double wake model (DWM) and Marion [3] extended

[1] http://www.wind-energy-the-facts.org/growth-of-wind-turbine-size.html

it to focus on the deep stall region. Later on, the model was modified to account for the dynamics of vortex shedding by Ramos-Garc´ıaet al. [4].

An unsteady version of a double wake model, capable of taking into account the dynamic effects of flow separation on airfoils was first developed by Vezza and Galbraith [6] three decadesago. This approach has been recently revisited by two researchgroups, Riziotis and Voutsinas [7] as well as Zanon et al. [8], which included an integral boundary solver to compute the separation location for flows around airfoils and carried out a large variety of dynamic stall simulations, with the airfoil pitching at a given rate. All three approachesmodeled the separated region with a set of time-updated vortex blobs, while different approaches were used to represent the airfoil contour as well as the handling of the first releasedwake panels.

A range of different authors have used vortex basedmethods to simulate cylinder flows. Sarpkaya and Shoaff [12] developed a method in which a doublet was used to represent the cylinder surface through a velocity-potential function, while vortex sheetswith constant vorticity were used to represent the downstream wake. Sarpkaya and Schoaff related the rate of vortex generation to the outer flow velocity at the separation location. Gerrard [15] was the first to use a discrete vortex approximation to model cylinder flows with the aid of experimental data. In an effort to better represent the cylinder surface, Kuwahara [13] used discrete vortices with images to satisfy the boundary condition at the body surface, which was divided in equal length partitions. In his work, Kuwahara related the strength of the nascent vortices to the Reynolds number. Roy and Badyopadhyay [14] were the first to use a panel method to represent the cylinder surface. However, the work was focused on steady state simulations, neglecting the dynamics of the vortex shedding behind the cylinder.

Contrary to the previous referred work, the present approach models the dynamic flows past a circular cylinder through a discrete representation of the cylinder

boundary, where the mechanism of vortex shedding is inherent to the model itself. The strength of the shedding vortex is calculated by combining two locally applied Kutta conditions and the Kelvin theorem of circulation conservation. The present solver emergesas an unsteady version of the Double Wake Model (DWM) developed by Ramos-Garc´ıa[2], and as such refereed to as USDWM (UnSteady Double Wake Model). The USDWM solver is employed to simulate subcritical, supercritical and transcritical flows around a circular cylinder. The aim of this work is for the first time to assessthe capability of this type of flow solvers to capture the changesin vortex shedding frequencies as well as body aerodynamic forces associated with the different flow states. Showing such detailed and dynamic capabilities of USDWM for the well-documented flow around cylinder, is the first step towards future applications in the simulation of separated flows around thick airfoils.

The results are compared and validated against classic experimental values by Schewe[5] as well as unsteady Reynolds averaged Navier-Stokes simulations (URANS) for three typical Reynolds numbers. The simulations spans the subcritical ($Re = 10^5$), supercritical ($Re = 10^6$), and transcritical ($Re = 7 \cdot 10^6$) range. The URANS results are obtained using OpenFOAM, an open source numerical flow solver for computational fluid dynamics [16]. URANS has been used to simulate flow around cylinders in numerous studies, *e.g.* Catalano et al. [19] and Ong et al. [20].

## 2. Numerical Models

Two different numerical models are employed in the present work and the two models are presented in the following: the panel code USDWM and OpenFOAM used for the URANS simulations.

*2.1. UnSteady Double Wake Model (USDWM)*

The freestream velocity field, $U_\infty$ , is changed once a body is placed in the flow. The body induces an additional velocity in the flow, so the total velocity in a point around the body is defined as

$$U = U_\infty + u \tag{1}$$

Assuming that the flow is incompressible, inviscid and irrotational, then the induced velocity $u$ can be expressed as the gradient of the potential field, $\nabla\varphi$, where $\varphi$ satisfies the Laplace equation. The general solution to the Laplace equation can be obtained through a source and vorticity distribution around the body. Moreover, the shed vorticity behind the solid body can be modeled with downstream converging vortex blobs. The velocity induced at any point in the domain can therefore be written using the superposition principle as follows,

$$u = u_\sigma + u_\gamma + u_{\gamma USEP} + u_{\gamma LSEP} + u_{\Gamma USEP} + u_{\Gamma LSEP} \tag{2}$$

where $u_\sigma$, $u_\gamma$ , are the velocities induced by the body's distributed sources and vortices. $u_{\gamma USE\ P}$ , $u_{\gamma LSE\ P}$ , are the velocities induced by the upper and lower separation vortex panels and $u_{\Gamma USE\ P}$ , $u_{\Gamma LSE\ P}$ , are the velocities induced by the upper and lower wake vortex blobs.

In the USDWM, the cylinder is discretized in N panels following the sketch in Figure 1. Each of the panels is represented by a linear distribution of vorticity, $\gamma_1$ to $\gamma_{N+1}$, which is piecewise continuous at the panel edges. Here, $\gamma_1$ is the trailing vorticity of the first panel and $\gamma_{N+1}$ is the leading vorticity of the last panel. The velocity field induced by the linear vorticity distribution from the $N$ panels can be written as follows,

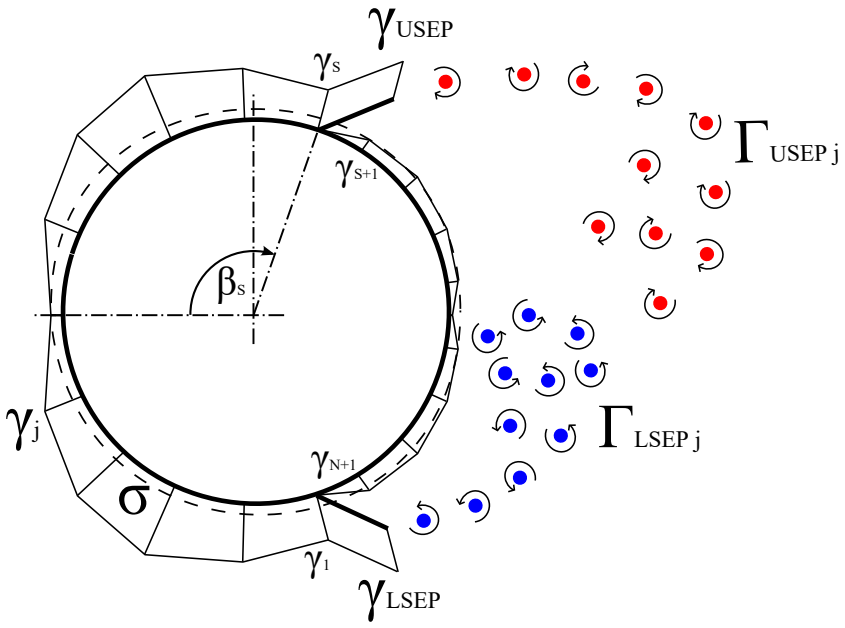


Figure 1: Sketch of the singularity distributions used in the USDWM to simulate the flow around a cylinder

$$u_\gamma = \frac{1}{2\pi}\sum_{i=1}^{N}\left[\frac{\gamma_i}{x_2}\left[(x_2 - x_p)(\theta_1 - \theta_2) + y_p \ln\frac{r_1}{r_2}\right] + \frac{\gamma_{i+1}}{x_2}\left[x_p(\theta_1 - \theta_2) - y_p \ln\frac{r_1}{r_2}\right]\right] \tag{3}$$

$$v_\gamma = \frac{1}{2\pi}\sum_{i=1}^{N}\left[\frac{\gamma_i}{x_2}\left[(x_p - x_2)\ln\frac{r_1}{r_2} + y_p(\theta_1 - \theta_2) - x_2\right] + \frac{\gamma_{i+1}}{x_2}\left[-x_p \ln\frac{r_1}{r_2} - y_p(\theta_1 - \theta_2) + x_2\right]\right] \tag{4}$$

where the different variables are defined in Figure 2.

The vortex strengths, $\gamma$, are used twice in the equations above, once as the leading vorticity of a given panel, $\gamma_L$, and once more as the trailing vorticity of that panel, $\gamma_T$. $\gamma_1$ and $\gamma_{N+1}$ are exceptions as they are only used once, as trailing vorticity of panel one and leading vorticity of panel $N + 1$, respectively.

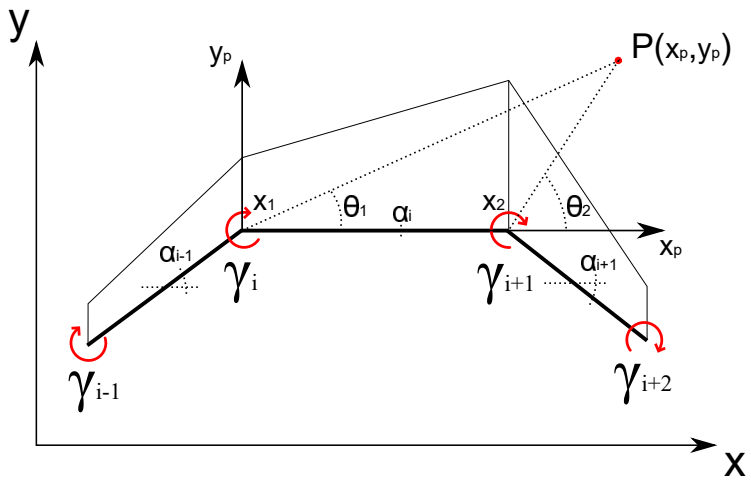


Figure 2: Sketch of the singularity used in the USDWM to simulate the flow around a cylinder

It is important to remark that the above velocities are written in panel coordinates, and therefore a transformation to global coordinates (x,y) using the panel angle $\alpha$ is necessary to compute the influence matrices. Furthermore, a constant source distribution, $\sigma$, is applied over the cylinder in order to close the system of equations.

The vorticity released at the upper and lower separation points is initially taken into account as two uniform panel distributions, $\gamma_{USEP}$ and $\gamma_{LSEP}$, which are convected into the wake as vortex blobs. The vortex blobs model the shear layers behind the body. The circulation of these vortices remain constant in time, satisfying Helmholtz's theorem [10]. The vortices are equipped with finite viscous cores in order to prevent an unstable behavior triggered by the point singularities. The finite

core prevents high velocities induced by a point vortex near its center. The velocity field induced by the *Nw* vortex blobs in the wake can therefore be obtained by desingularizing the Biot-Savart equation with the Lamb-Oseencore model as follows,

$$u_\Gamma = \frac{1}{2\pi} \sum_{i=1}^{Nw} \Gamma_i \frac{y_i - y}{r^2} \left[ 1 - e^{-\frac{r^2}{r_c^2}} \right] \tag{5}$$

$$v_\Gamma = \frac{1}{2\pi} \sum_{i=1}^{Nw} \Gamma_i \frac{x_i - x}{r^2} \left[ 1 - e^{-\frac{r^2}{r_c^2}} \right] \tag{6}$$

where $r_c$ is the viscouscore radius, which for this work is maintained constant in time. A core growth model could be applied as a simple way to model viscous dissipation by increasing the core radius in time, seeAnanthan and Leishman [18]. $r_c$ has been set to 4% the cylinder diameter in the present work.

A total of N+4 unknownshaveto be determined, namely $\gamma_1$ to $\gamma_{N+1}$, $\gamma_{USEP}$ and $\gamma_{LSEP}$ and $\sigma$. Hence, the flow around a cylinder for a given distribution of flow singularities can be modeled using the following system of equations:

- Eq. 1-N: Neumann no-penetration condition at the cylinder surface, stating that the normal velocity at each one of the panel control points (center of the panels) must be equal to zero,

$$U_i \cdot n_i = 0, \quad i = 1,\ldots,N \tag{7}$$

  Expanding the above equation to take into account the influence of the freestream, the body's motion and all the induced velocities from both the body and the wake singularities gives:

$$\sigma A_i + \sum_{j=1}^{N+1} C_{ij}\gamma_j + E_{iU}\gamma_{USEP} + E_{iL}\gamma_{LSEP} + \sum_{j=1}^{N_w} (G\Gamma_j \cdot n_i) + U_\infty \cdot n_i + U_{body} \cdot n_i = 0, \quad i = 1,\ldots,N \tag{8}$$

where $A$ is the sourcenormal induction vector, $C$ is the linear vorticity normal induction matrix, $E$ is the separation panels normal induction vector and $G\Gamma_j$ represents the velocity induced by the vortex blobs in the wake. Furthermore, $U_\infty$ and $U_{body}$, are the freestream and the body's velocity respectively.

Note that the local coefficients in the linear vorticity normal induction matrix are split into the velocity induced by the leading and trailing vortex of a panel as follows,

$$C_{ij} = (u_{ij+1,L} + u_{ij,T})(-sin\ \alpha_i) + (v_{ij+1,L} + v_{ij,T})(+cos\alpha_i) \tag{9}$$

where $u_{ij+1,L}$ , $v_{ij+1,L}$ represent the velocity components induced by the vortex $\gamma_{j+1}$ with unit strength acting as the leading vortex of panel $j$ , and $u_{ij,T}$ , $v_{ij,T}$ represent the velocity components induced by the unit strength vortex $\gamma_{j-1}$ as trailing vortex of panel $j$ .

- Eq. N+1: unsteady Kutta condition [11], stating that the flow must leave the cylinder at the lower separation point

$$\gamma_1 + \gamma_{N+1} = \gamma_{LSEP} \tag{10}$$

- Eq. N+2: zero vortex strength at the station N+1, which combined with the unsteady Kutta condition forces all the vorticity in the lower attached flow region to be transferred into the wake, satisfying Helmoltz's theorem of continuity of vorticity,

see Figure 3.

$$\gamma_{N+1} = 0 \tag{11}$$

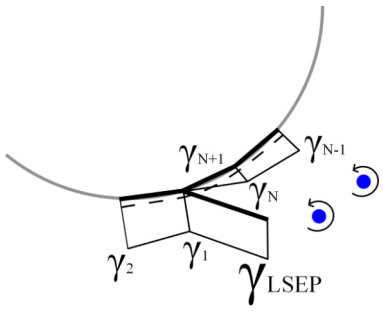


Figure 3: Sketch of the enforced condition at the lower separation location

- Eq. N+3: an equivalent condition has to be applied at the upper separation location in order to enforce the separation zone to start with a zero vorticity distribution. Therefore, modeling the transfer of the vorticity from the upper attached flow region, $\gamma_S$, into the wake. The common location of vortices 1 and $N + 1$ made the application of this condition straight forward for the lower separation location. However, this is not the case for the upper location, where this condition has to be enforced by modifying the induction coefficients for the panel $S$. Here, the trailing vorticity is set to 0, as shown in Figure 4,

$$C_{iS} = (u_{iS+1,L} + 0)(-sin\ \alpha_i) + (v_{iS+1,L} + 0)(+cos\,\alpha_i) \tag{12}$$

Notice, that the modification above also has to be applied to the coefficients in the tangential induction coefficients matrix, $D$.

Following this reasoning, the vortex strength at the upper separation panel is equal to the leading vorticity of the $S - 1$ panel, $\gamma_S$, which still satisfies the Helmholtz's theorem of continuity of vorticity,

$$\gamma_{USEP} = \gamma_S \tag{13}$$

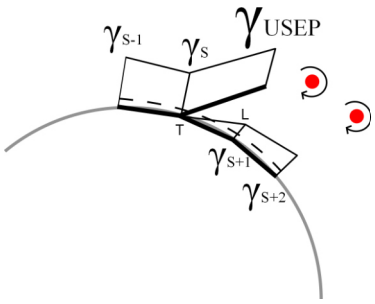


Figure 4: Sketch of the enforced condition at the upper separation location

- Eq. N+4: Kelvin's theorem [9] assuresthat the circulation will be conserved,and it is applied as follows,

$$\gamma^t_{USEP}\Delta^t_{USEP} + \gamma^t_{LSEP}\Delta^t_{LSEP} = \Gamma^t_B - \Gamma^{t-1}_B \tag{14}$$

where $\Delta^t_{USEP}$, $\Delta^t_{LSEP}$ are the lengths of the upper and lower separation panels, respectively, at a time step t. $\gamma^t_{USEP}$, $\gamma^t_{LSEP}$ are the panel strengths and $\Gamma^t_B$, $\Gamma^{t-1}_B$ are the body's total circulation at time step t and t-1, respectively.

The system of equations is closed and all the unknowns can be determined. The velocities induced by the vortex blobs in the wake are included in the right hand side of the system, where their strength remains constant in time, unless they are merged by the coalescencecriteria or the far wake model.

After solving the system of equations, the lengths and angles of the upper and lower separation panels are calculated as follows,

$$\Delta_{USEP} = \frac{|\gamma_{USEP}|}{2}\Delta t \tag{15}$$

$$\Delta_{LSEP} = \frac{|\gamma_{LSEP}|}{2}\Delta t \tag{16}$$

$$\theta_{USEP} = tan^{-1}\left[\frac{v_{USEP}}{u_{USEP}}\right] \tag{17}$$

$$\theta_{LSEP} = tan^{-1}\left[\frac{v_{LSEP}}{u_{LSEP}}\right] \tag{18}$$

through an iterative procedure. The angles and lengths of the separation panels are used to update the system and recalculate the singularity strengths. This procedure is repeated until convergence,which is obtained once the residual value of $\Delta_{USEP}$, $\Delta_{LSEP}$, $\theta_{USEP}$, $\theta_{LSEP}$ as well the total circulation, $\Gamma_B$, is lower than a threshold. In all the simulations presented in this article the maximum residual has been set to $10^{-4}$.

Once convergence is satisfied, the tangential velocity, $up_i$, is calculated in panel co-ordinates at each one of the panel collocation points by superposition of the different singularities, the freestream and the body's motion,

$$up_i = \sigma B_i + \sum_{j=1}^{N+1} D_{ij}\gamma_j + F_{iU}\gamma_{USEP} + F_{iL}\gamma_{LSEP} + \sum_{j=1}^{N_w} (G\Gamma_j \cdot t_i) + U_\infty \cdot t_i + U_{body} \cdot t_i, \quad i = 1,\ldots,N \tag{19}$$

where $B$ is the source tangential induction vector, $D$ is the linear vorticity tangential induction matrix, $F$ is the separation panels tangential induction matrix.

The surface pressure coefficient, $C_p$, is calculated using the unsteady Bernoulli equation, including a pressure correction for the separated region. This area is treated as isolated from the rest of the flow, and therefore an increase in total pressure over that at the outer flow has be taken into account in the form of a pressure jump,

$$C_p = 1 - \frac{up^2}{U_\infty^2} - \frac{2}{U_\infty^2}\frac{\partial \varphi}{\partial t} - \frac{2}{U_\infty^2}\Delta h \tag{20}$$

where $\Delta h$ is the total pressure jump at the interface of the two wake sheets, which only adopts a non-zero value inside the wake region, see Maskew and Dvorak [1]. The pressure jump can be expressed as the difference between the pressure heads on both sides of the wake sheets, see Zanon et al. [8],

$$\Delta h = h_1 - h_N = \frac{\partial}{\partial t}[\varphi_1 - \varphi_N] + \left( up_1^2 - up_N^2 \right) \tag{21}$$

The lift and drag values are calculated by integrating the pressure coefficient around the cylinder. However, the influence of skin friction, and therefore viscous drag, is not included in the USDWM model.

Once the solution is obtained at time t, the existing vortices are convected downstream to their new positions using a first order Euler scheme,

$$\mathrm{r}_j^{t+1} = \mathrm{r}_j^t + \mathrm{u}\left( t^{t+1} - t^t \right) \tag{22}$$

The upper and lower separation panels are converted into vortex blobs and convected downstream using the same scheme as above.

### *2.1.1. Additional Considerations for the USDWM model*

The separation location is critical for the model and can be determined by two different approaches.

The first method is to force the flow to separate at a specific location in both the upper and lower sides of the cylinder. This approach is used in the present work. The information of the actual separation location can be obtained from experimental data or from higher fidelity models, *e.g.* CFD.

The second approach is to employ a boundary layer solver, which solves the integral

boundary layer equations in a downstream marching manner until separation is found. This approach, which is more complex and often shows unstable behavior due to the mathematical properties of the boundary layer equations, is commonly used for airfoil simulations, *e.g.* Riziotis and Voutsinas [7] and Zanon et al. [8].

In order to avoid the non-physical phenomena of surface penetration by discrete vortex blobs, and at the sametime fulfil Kelvin's theorem of conservationof circulation, the vortex blobs that enter the cylinder contour are reflected towards the outer flow in the direction perpendicular to the closest discrete panel, as sketched in Figure 5.

To avoid unphysical clusters of vortex blobs in the vicinity of the cylinder, a virtual boundary with constant thickness has been created around the cylinder, see Vezza and Galbraith [6]. A vortex blob located between the cylinder surface and this boundary is automatically moved to the edge of the boundary, as seenin Figure 5.

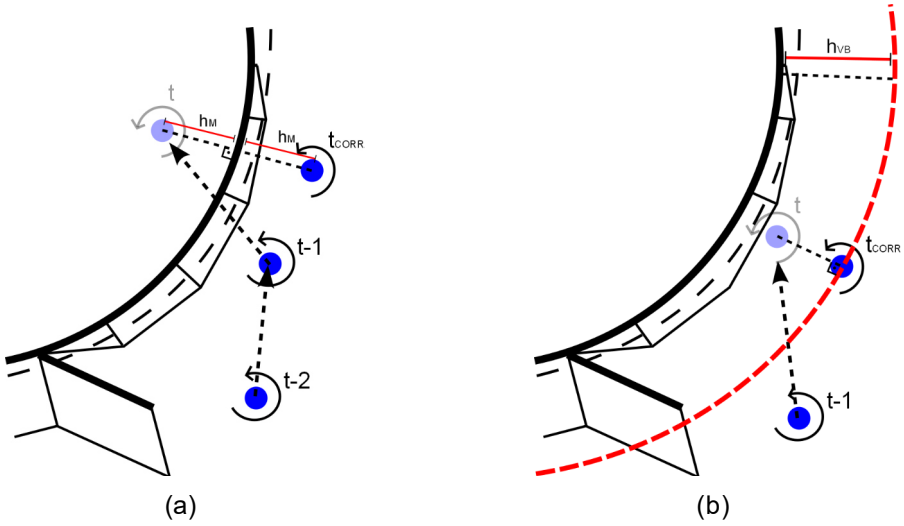


Figure 5: Sketch of (a) vortex blob reflection (b) virtual boundary around the cylinder surface

Furthermore, a coalescencecriteria has been introduced in the near wake region to minimize the number of Biot-Savart interactions. The coalescencecriteria essentially merges two vortex blobs of opposite sign into one, when they are located close enough to each

other. The coalescenceradius, $r_{cc}$, needsto take a value of the same order of magnitude as the time step.

A far wake model has been introduced in order to limit the increasing computational time required by the USDWM model due to the growing number of vortex blobs in time. Once the maximum number of vortex blobs has been reached, the three blobs located further downstream in the flow domain are merged into one. In this way, the number of vortex blobs is maintained constant at the same time as the Kelvin theorem remains satisfied The location of the merged vortex is calculated as follows,

$$x_{farwake} = \frac{x_A|\Gamma_A| + x_B|\Gamma_B| + x_C|\Gamma_C|}{|\Gamma_A| + |\Gamma_B| + |\Gamma_C|} \tag{23}$$

$$y_{farwake} = \frac{y_A|\Gamma_A| + y_B|\Gamma_B| + y_C|\Gamma_C|}{|\Gamma_A| + |\Gamma_B| + |\Gamma_C|} \tag{24}$$

The circulation of the merged vortex is obtained as follows,

$$\Gamma_{farwake} = \Gamma_A + \Gamma_B + \Gamma_C \tag{25}$$

### *2.1.2. Simulation Setup*

The cylinder surface is divided into 70 panels, the free-stream velocity, $U_0$, is 1 m/s and the diameter, $D$, is fixed to 1 m. The time step is set to 0.028 s, which is in the order of the averagepanel length (0.028$D$) times $U_0$. The flow past the cylinder has been simulated for 300 seconds. The viscous core has been set to be equal to the average panel length, analogousto a Courant-Friedrichs-Lewy (CFL) condition of unity. In order to avoid vortex accumulation, the virtual boundary thickness is set equal to the viscous core radius. Moreover, the maximum number of vortex blobs in the wake has been fixed to 1000 and a coalescencecriterion has been used in order to reduce the number of vortex blobs in the near wake.

The coalescenceradius between particles is fixed to 0.04 and all vortices located less

than two diameters downstream of the trailing edge are candidates for merging. The far wake model is used to maintain the total amount of vortex blobs below the given maximum. The separation point at the surface of the cylinder, $\beta_s$, is obtained from the experimental data of Schewe[5]. $\beta_s$ is fixed in the USDWM simulations to 80, 140 and 110 degrees for the subcritical, supercritical and transcritical cases, respectively.

### *2.2. Unsteady RANS simulations*

Simulations are also performed using the open source CFD toolbox OpenFOAM as an additional validation of the results. A standard $k-$ □formulation is used to model the turbulence for the cases at $Re = 10^6$ and $7 \cdot 10^6$. For the subcritical case at $Re = 10^5$ a $k-\omega SST$ model is used for its performance and its low sensitivity to the initial conditions following Sarlak et al. [25]. Crank-Nicolson time discretization is used for the temporal derivatives and the gradient, Laplacian and divergence terms are solved using Gauss linear, Gauss linear corrected, and Gauss linear discretization schemes, respectively.

The PIMPLE algorithm is used to solve the Navier-Stokes equations and the simulations are advanced in time using a variable time step, which ensures that the Courant number is kept below 0.5. Computations are run in parallel using the ”scotch” domain decomposition – as it requires no geometric input from the user and attempts to minimize the number of processor boundaries [16]– on 8 cores for 300 non-dimentional time units ($tU_0/D$), i.e. for $D = 1m$ and $U_0 = 1m/s$ it corresponds to $300s$ as in the USDWM simulations.

The computational domain is divided into inlet, outlet, cylinder, top, and bottom. The computational domain measures $20D \times 25D$ in the vertical and streamwise directions. Figure 6 shows a closeup of the computational grid in the vicinity of the cylinder used for the CFD simulations.

Mesh refinement has been performed (results not shown) in order to ensure the quality of the CFD results. The mesh consists of 60,700 cells with 392 cells surrounding the cylinder. For the subcritical ($Re = 10^5$) case, the wall is resolved, *i.e.* a nondimensional grid spacing of $y^+ \approx 1$ is used near the cylinder. For the supercritical and transcritical

cases,however, near wall modeling is applied corresponding to an average nondimensional grid spacing of $y^+ \approx 50$. For more information about grid spacing the reader is referred to Sarlak [24].

A uniform reference velocity is imposed at the inlet and the pressure is set to ”zero-Gradient”. The velocities are set to ”zeroGradient” while the pressureis set to zero at the outlet. A no slip boundary condition is used for the velocity and the pressure value is set to ”zeroGradient” at the cylinder boundary. Finally, a symmetry boundary condition is applied for both velocity and pressureat the top and bottom boundaries. Boundary values for turbulence model terms ($k$ and □) are symmetry condition for the top, bottom, and outlet boundaries. The applied boundary conditions at the cylinder are similar to those outlined in Ong et al. [20].

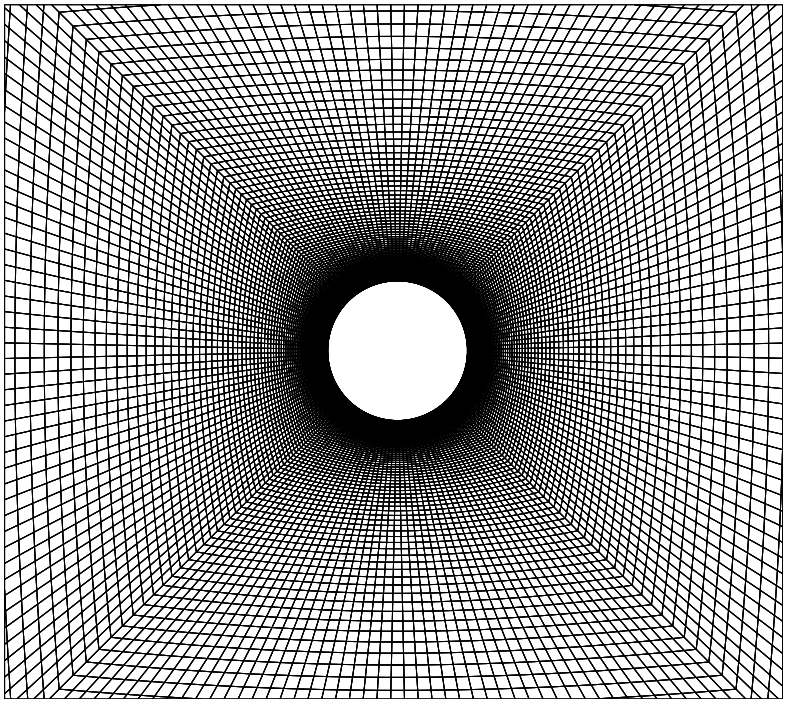

Figure 6: A close snapshot of the computational grid used for the URANS computations.

## 3. Results

The presented results and computed quantities are shown once the initial transients have left the computational domain.

### *3.1. Cylinder Flow Visualizations*

Instantaneous flow visualizations from USDWM are shown in Figure 7 for all three Reynolds numbers. Red and blue dots show vortex blobs released from the upper and lower surfaces, respectively. The large red circle at the far edge of the domain corresponds to the far wake model, which gathers the effect of the removed vortex blobs. The typical vortex shedding behind a cylinder is clearly visible with alternating regions of red or blue vorticity. The different locations of the separation points are also clearly seen in the three different regimes. The location of the separation point directly affects the size and occurrence of the shed vortices. The shedding frequency is increased as the separation angle, $\beta_s$, increases. Similar tendencies are seen in Figure 8, which shows the streamwise velocity contours from the URANS simulations. The exact location of separation is not as clearly detected, but the influence on the wake development is clearly seen as regions of high and low velocity moves downstream.

Figure 9 shows the instantaneous lift coefficients for the three regimes extracted from the USDWM results. As expected, the frequency of the lift oscillation increases with the increase in $\beta_s$. It is also seen how the amplitude of the oscillations changes, which resembles the unsteady nature of experiments or more advanced LES simulations, although with less variation, see Catalano et al. [19]. Such change in amplitude is not captured in the URANS simulations, which yields periodic oscillations with constant amplitudes (not shown for brevity).

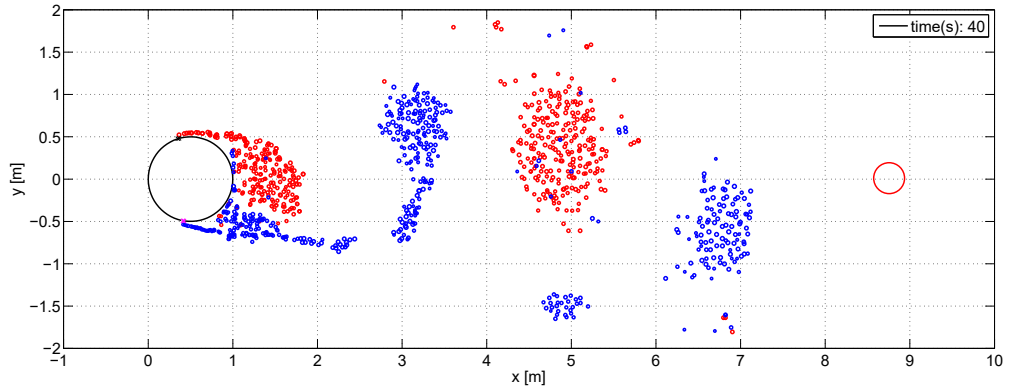


(a)

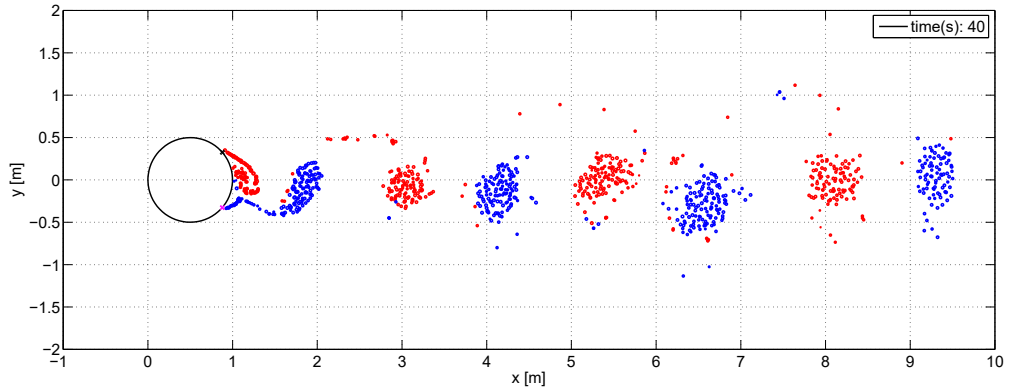


(b)

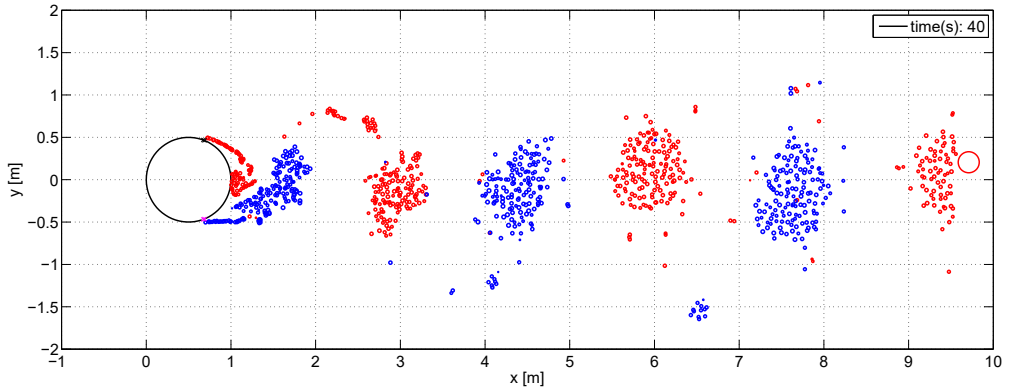


(c)

Figure 7: USDWM simulation of the flow past a cylinder, instantaneous flow visualization at t = 40 s (a) subcritical, (b) supercritical (c) transcritical flow .

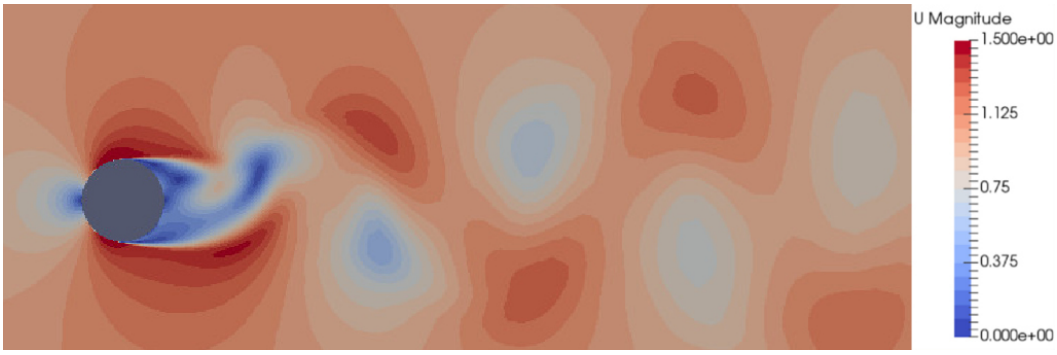


(a)

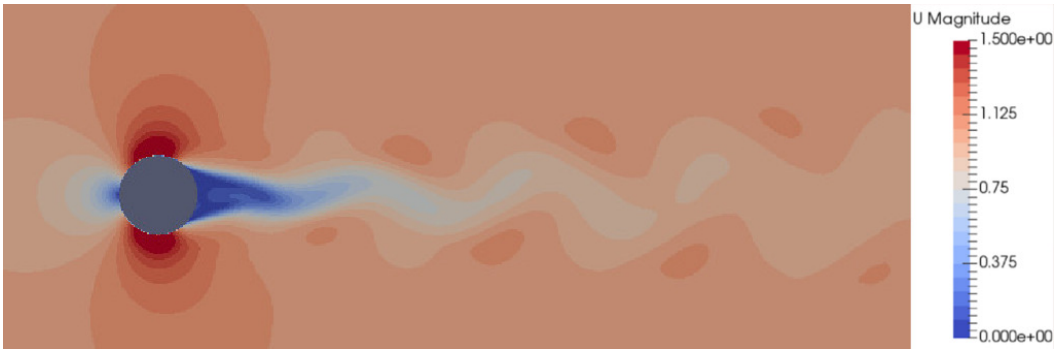


(b)

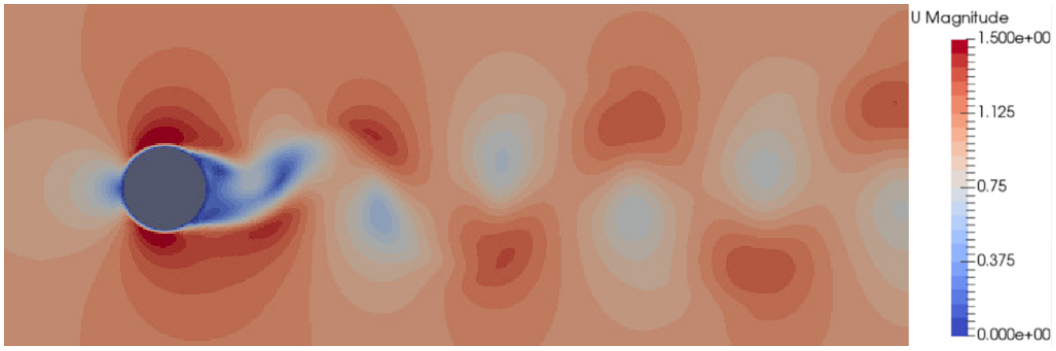


(c)

Figure 8: OpenFOAM-URANS simulation of the flow past a cylinder, instantaneous flow visualization of the velocity magnitude contours for the a) subcritical, b) supercritical, and c) transcritical flow regimes

### *3.2. Cylinder Strouhal Frequencies*

The energy spectra of these lift coefficients are calculated and shown in Figure 10. The filtered and non-filtered spectrums are shown and the peak frequencies corresponding to the Strouhal frequencies for the three flow regimes are marked. Figure 11 compares the Strouhal frequencies derived from the USDWM and URANS simulations with the experimental data by Schewe[5]. The Strouhal frequencies derived from the USDWM is marked by lines as the Reynolds number was indirectly derived by selecting the separation location from the experimental.

Both the USDWM and URANS are capable of accurately capturing the Strouhal frequency in the subcritical and transcritical Reynolds regime. However, the shedding frequency is underpredicted for the supercritical case. This discrepancy could be explained by the two-dimensionality of the simulations. The three-dimensional nature of the vortex shedding in the experiments generate vortex structures in the spanwise direction, which increase the interaction between the vortex sheets, hence the shedding frequency. This effect is particularly pronounced when the vortex sheets are close to each other.

### *3.3. Cylinder Drag and Pressures Coefficients*

Figure 12 shows the drag coefficients for all three regimes for USDWM and URANS. Surprisingly, the comparison of the drag coefficients is opposite to the Strouhal frequencies. Here, both models perform better for supercritical flow, while the drag coefficient is underpredicted for subcritical and overpredicted for transcritical. USDWM performs slightly worse than URANS for subcritical, but better for transcritical. The discrepancy is probably due to that USDWM does not include the viscous(or friction) drag, while the pressure drag dominates for higher Reynolds numbers, where the estimated drag coefficient from USDWM matches well. The discrepancy can also be related to the choice of

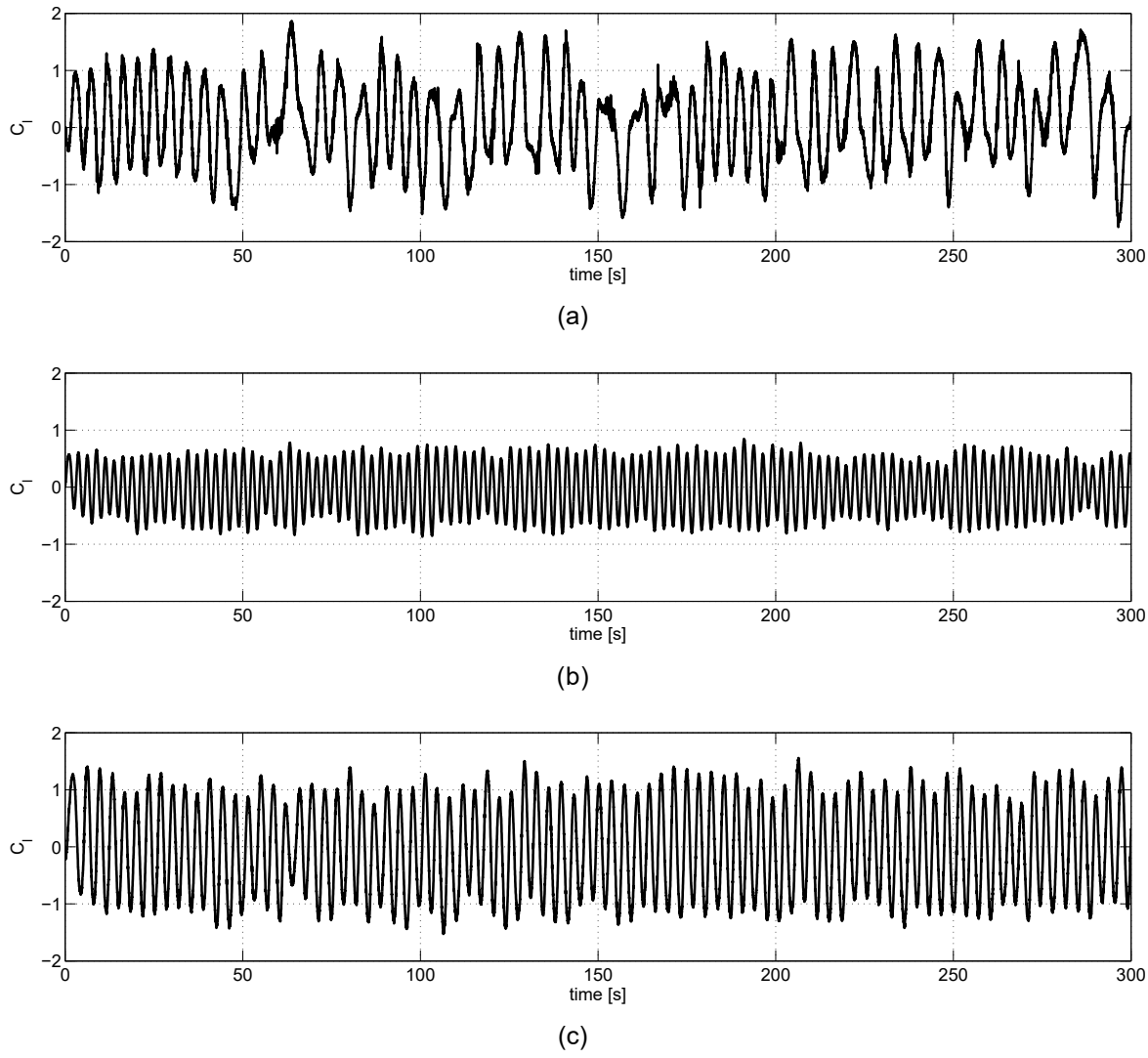


Figure 9: USDWM simulation of the flow past a cylinder, lift coefficient time signal (a) subcritical, (b) supercritical (c) transcritical flow

separation location, as will be discussedin further details in Section 3.4. The discrepancy in the URANS simulations are most likely related to the location of the separation point, which is notoriously difficult to predict particularly for relatively low Reynolds numbers. However, the overall behavior of the three regimes is captured correctly.

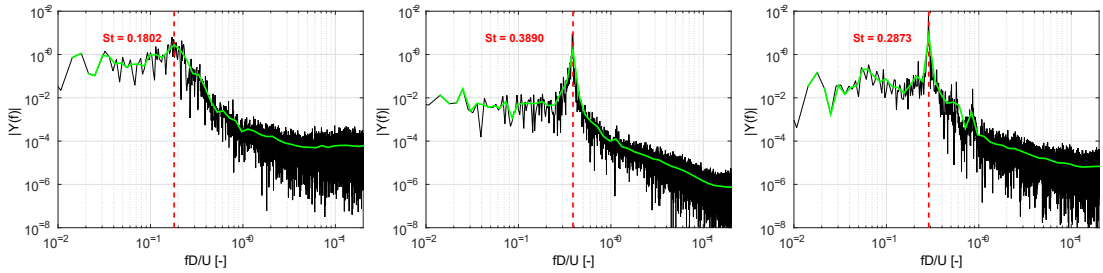


(a) (b) (c)

Figure 10: USDWM simulation of the flow past a cylinder, filtered(green lines) and non-filtered(black lines) energy spectra of the lift coefficient (a) subcritical, (b) supercritical and (c) transcritical Reynolds. .

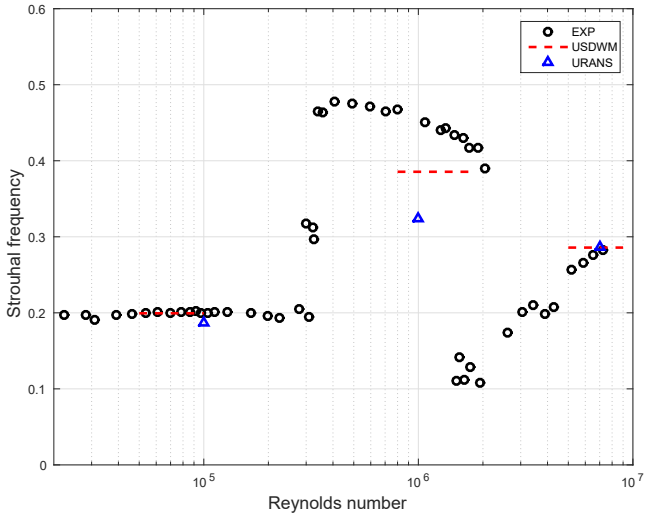


Figure 11: Comparison of Strouhal frequency computed using the USDWM(red broken lines) and URANS(blue triangles) against experimental data(black circles) from Schewe[5].

The average pressure coefficients at the cylinder surface are shown in Figure 13 for the two models. There is an excellent match between the two models for both supercritical and particularly for transcritical regimes. There are minor discrepancies in the separation region, where USDWM yields an almost constant pressure distribution while increasing slightly at the back of the cylinder. This can be explained by an accumulation of vorticity in the near wake, which is critical in two-dimensional flow simulations due to the absence

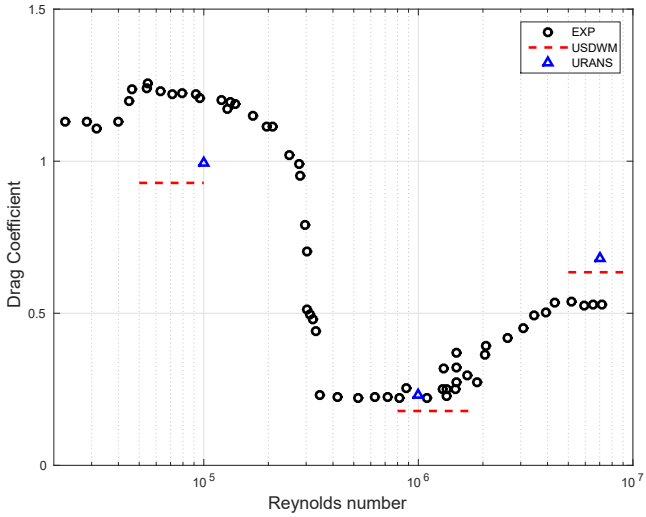


Figure 12: Comparison of the drag coefficient computed using the USDWM (red broken lines) and URANS (blue triangles) against experimental data (black circles) from Schewe[5].

of three-dimensional effects that help vortex diffusion. It is worth to note here that the inclusion of a viscous core growth model or a random walk, as a crude way of modeling diffusion, lowers this unwanted effect.. The difference is larger for the subcritical regime. The USDWM is also less continuous around the separation location with minor jumps in the pressure coefficient due to its coarser surface mesh discretization. Interestingly, the $C_p$-distributions are not symmetric over the surface of the cylinder for either model, which could explain the underprediction of the overall drag coefficient as shown in Figure 12.

### *3.4. Cylinder Parametric Study*

The USDWM only depends on the location of the separation point, and therefore a total of 17 simulations have been carried out with the USDWM solver to study the drag coefficient and Strouhal frequency variation as function of the separation location. $\beta_s$ has been varied from 70 to 150 degrees, with steps of approximately 5 degrees.

USDWM presents a smooth transition in both drag coefficient and Strouhal number between 75 − 135 degrees, while it experiences a non-physical behavior in the extreme

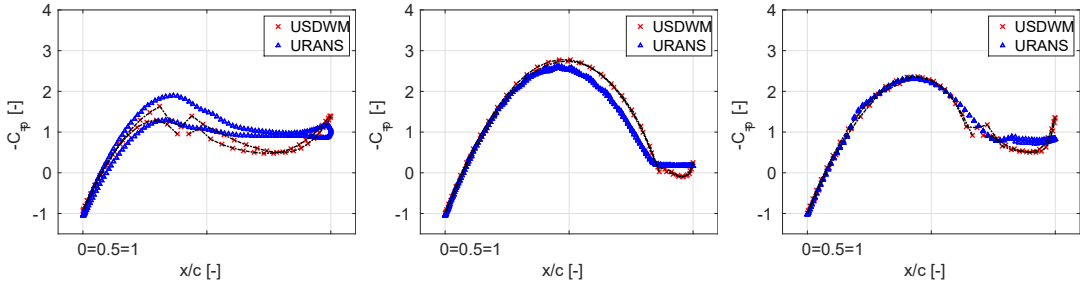


Figure 13: Average value of the surface pressure coefficient ($C_p$) from simulation time 200 to 300 seconds(a) subcritical, (b) supercritical and (c) transcritical Reynolds.

cases of 70 degrees and above 145 degrees, see Figures 14. These separation locations are extreme cases,out of the range of the actual fluid flow physics based on the experimental data by Schewe[5]. These cases(markedin green) are simulated to test the abilities of the flow solver. Separation locations above 140 degreesresults in an unstable region, where the vortex structures behind the cylinder transition to a much higher Strouhal frequency (0.8) and the mean drag coefficient approaches zero. The three URANS results are also plotted, as it shows the same dependency on separation location. The drag coefficient decreaseand the Strouhal frequency increase as the separation angle is increased.

Finally, the URANS simulations are used to validate the separation locations used in USDWM. Figures 15 showthe skin friction as function of azimuthal angle for the transcritical regime. The separation location is taken, where the skin friction becomespositive, i.e. the skin friction changesdirection on the cylinder surface as the flow separates. The skin friction is plotted for two or three different times to visualize how the separation location is not necessarily a constant location, but rather changeswith time. The most dynamic separation location is found in the transcritical, where the separation location changefrom 128.3 to 123.8 degreesand back within 10$s$. This is not the case for the subcritical and supercritical regimes, where the separation is almost constant at 87 and 137.3 degrees,re-

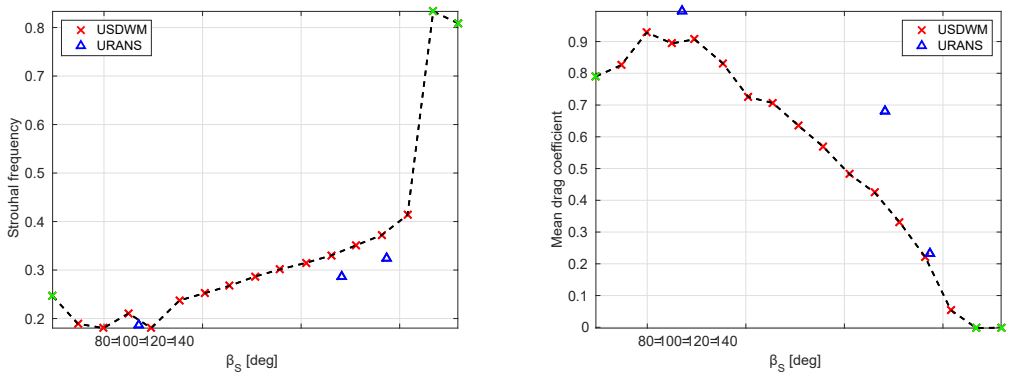


(a) (b)

Figure 14: Predicted quantities as function of the separation location in degrees, $\beta_s$, (a) Strouhal frequency (b) Drag coefficient.

spectively. These are different to the separation locations derived from experiments of 80, 140 and 110 degrees used in USDWM, in particular for the transcritical case. Using Figure 14, it can be seen how there would be minimal change in the Strouhal frequency and drag coefficient for subcritical and supercritical. However, using the URANS derived separation location would result in a decreased drag coefficient and increased Strouhal frequency, which would improve the prediction of the drag coefficient, but still remains comparable in terms of Strouhal frequency.

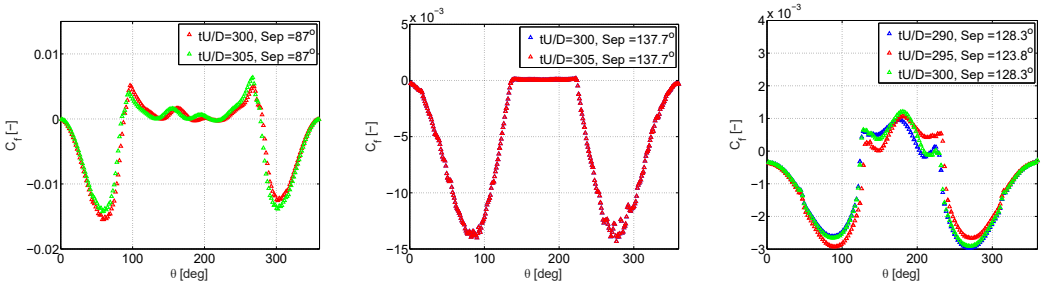


(a) (b) (c)

Figure 15: Skin friction distribution at different time steps in the (a) subcritical, (b) supercritical and (c) transcritical regime.

### *3.5. Cylinder Wake Analysis*

The wake development behind the cylinder as computed by USDWM is examined in the following. The mean streamwise velocity, vertical velocity, and Reynolds stresses($< u^0 v^0 >$) for the subcritical, supercritical, and transcritical Reynolds numbers are shown in Figure 16. The subcritical results are compared to experimental values taken from Cantwell et al. [23]. The mean streamwise velocity profiles are compared at 1.5$D$ and 3.0$D$, with the 1.25$D$ location included as additional reference. As seen, the shape and level of the mean streamwise velocity is well captured by USDWM, although the wake recovery is slightly slower than the experimental wake recovery. A similar trends is seen for the vertical velocity profiles, while the Reynolds stress is slightly overpredicted by USDWM. However the location of the peaks is captured by USDWM, and having comparable second order statistics show how USDWM is capable of capturing the correct dynamics of the flow behind a cylinder. The velocity profiles are also shown for supercritical and transcritical Reynolds numbers, despite the lack of experimental data for comparison. The narrower wake for the supercritical regime is clearly seen, which results in a smaller wake deficit in the streamwise velocity and a steeper slope in the vertical velocity profile. However, the wake recovery is initially even faster for the transcritical case, although the wider wake yields a smaller slope in the vertical profile. However, the biggest difference is seen in the magnitude of the Reynolds stress for the supercritical regime is only about 1/3 of the subcritical regime and 1/2 of the transcritical regime.

### *3.6. Airfoil Simulations*

The 21% thick airfoil FFA-W3-211 is used for further validation of USDWM. The experimental campaign used herein for the validation was carried out in the low speed wind tunnel L2000 [21] at the Royal Institute of Technology, Stockholm. Measurements were performed at a Reynolds number of $1.8 \cdot 10^6$ and a turbulence intensity of 0.15%. Simulations with the USDWM have been carried out at four different angles of attack: 12, 15, 19 and 23 degrees. The separation location has been calculated with the in-house

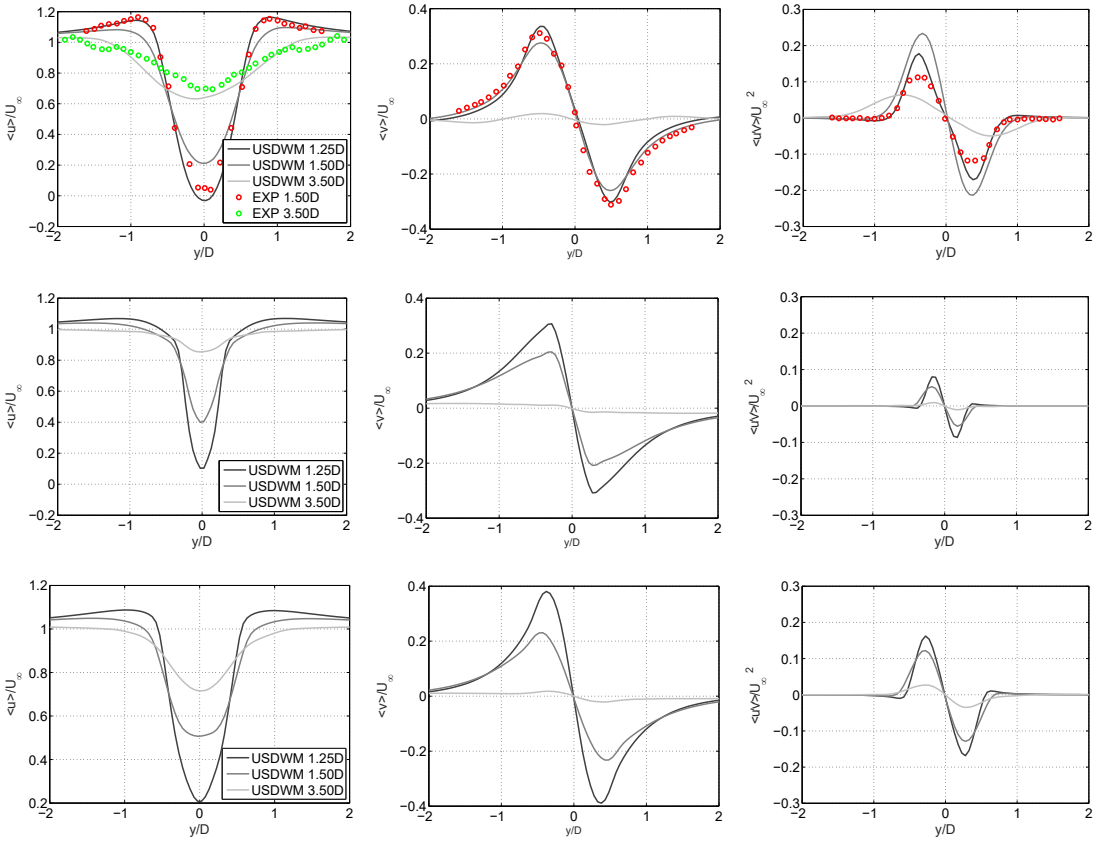


Figure 16: Vertical profiles of the (left) mean streamwise velocity, (center) mean vertical velocity, and (right) Reynolds shear stress at a (upper) Subcritical, (middle) Supercritical, and (lower) Transcritical Reynolds number. Experiments from [23] included for the subcritical regime.

viscous-inviscid solver Q3UIC [22]. Q3UIC solves the integral form of the boundary layer equations using a strong viscous inviscid coupling procedure. Figure 17 shows the predicted aerodynamic forces (lift and drag) compared to experiments. The highly unstable and dynamic post-stall is captured very well by USDWM as indicated by the red error bars. Clearly, the variability in the lift and drag forces increases with increasing angle of attack (AoA). The instantaneous and average lift coefficients for $AoA = 12$ and $AoA = 19$ degrees are shown in Figure 18, where there is an initial transient as the wake behind the airfoil develops downstream.

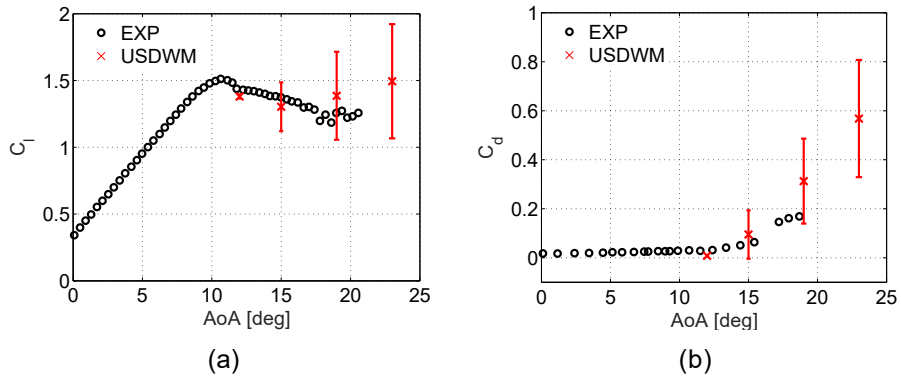


Figure 17: Comparison of the USDWM computed aerodynamic forces over the FFA-W3-211 airfoil section against average experimental data (a) lift and (b) drag coefficients.

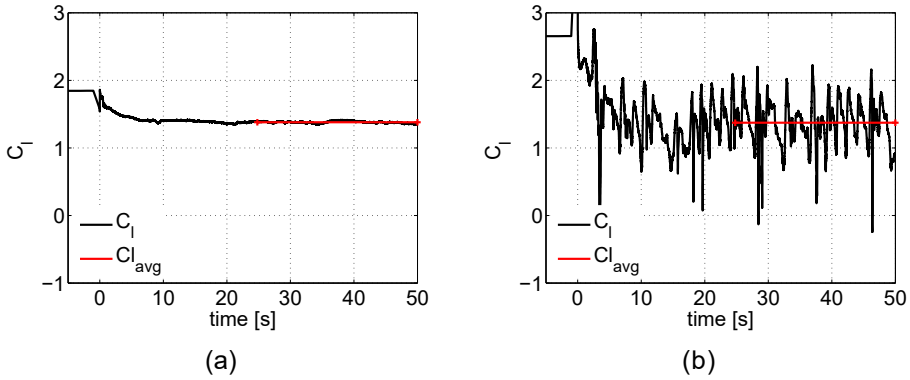


Figure 18: USDWM simulation of the flow past the FFA-W3-211 airfoil at a Reynolds number of $1.8 \cdot 10^6$. Instantaneous(black lines) and average(red lines) value of Cl at angles of attack (a) 12 and (b) 19 degrees.

## 4. Conclusion

In this article, the flow past a cylinder was simulated using the newly developed Unsteady Double Wake Model (USDWM) for the subcritical, supercritical and transcritical regimes. The model was validated against experimental data and URANS simulations in terms of flow visualizations, Strouhal frequencies, wake profiles, drag and pressure coefficients. The results generally showed a good agreement between USDWM, URANS, and

experiments. USDWM is shown to be capable of accurately capturing the dynamics of the flow as well as the changes in shedding frequencies and drag coefficients for the three different regimes. The comparison between USDWM and URANS in terms of pressure distributions around the cylinder was also good. Furthermore, the capability of the model was tested for a large range of separation locations, which revealed how USDWM yields continuous results with a slightly increasing Strouhal frequency and decreasing drag coefficient with increasing separation location, as expected due to the increased vortex interaction. Furthermore, USDWM correctly predicts unphysical behavior, when the enforced separation location exceedsthe physical range. The separation location was also extracted from the URANS simulations, which were slightly different to the experimentally derived values. Applying the separation locations from the URANS would slightly improve the drag coefficient for the transcritical regime. The shape of the velocity and Reynolds stress profiles in the wake is captured well for the subcritical regime compared to experiments, although the magnitude is slightly underpredicted. The wake development was also shown for the supercritical and transcritical regime. Finally, USDWM was applied to a wind turbine airfoil, and was shown to capture the average aerodynamic forces in the post-stall region very well as compared to experiments.

## 5. Acknowledgements

The authors would like to acknowledge the support from the European Union's Seventh Programme for research, technological development and demonstration for the project 'AVATAR: AdVanced Aerodynamic Tools for lArge Rotors'(FP7-ENERGY-2013-1/no. 608396).

## References

[1] B. Maskew and F. A. Dvorak 1978 The Prediction of Clmax Using a Separated Flow Model *Journal of the American Helicopter Society, Vol. 23, Issue 2, pp. 2-8*

[2] N. Ramos-Garc´ıa2011 Unsteady viscous-inviscid interaction technique for wind turbine airfoils *PhD. Thesis, Technical University of Denmark, Department of Mechanical Engineering, ISBN 978-87-90416-53-9*

[3] L. Marion, N. Ramos-Garc´ıaand J. N. SørensenAugust 2014 Inviscid Double Wake Model for Stalled Airfoils *The Science of Making Torque from Wind. IOP Publishing. Journal of Physics: Conference Series 524 (2014) 012132*

[4] N. Ramos-Garc´ıa, A. Cayron and J. N. SørensenJuly 2015 Unsteady Double Wake Model for the Simulation of Stalled Airfoils *Journal of Power and Energy Engineering, Proceedings of the 5th Conference on New Energy and Sustainable Development.*

[5] G. Schewe1983 On the Force Fluctuations Acting on a Circular Cylinder in Crossflow from Subcritical to Transcritical Reynolds Numbers *J. Fluid Mech. 133, 265*

[6] M. Vezza and R.A.McD. Galbraith 1985 An Inviscid Model of Unsteady Aerofoil Flow with Fixed Upper Surface Separation. *International Journal for Numerical Methods in Fluids, 5, 577-592*

[7] V. A. Riziotis and. S. G. Voutsinas 2007 Dynamic Stall modelling on airfoils based on strong viscous-inviscid interaction coupling. *International Journal for Numerical Methods in Fluids, 56, 185-208*

[8] A. Zanon, P. Giannattasio, C. J. S. Ferreira 2013 A vortex panel model for the simulation of the wake flow past a vertical axis wind turbine in dynamic stall. *Wind Energy, 16, 661-680*

[9] L. M. Milne-Thomson 1952Theoretical Hydrodynamics. MacMillan and Co. Ltd., London, 2nd Edition, p.77

[10] L. M. Milne-Thomson 1966 Theoretical Aerodynamics. Dover Publications Inc., New York, 4th Edition, pp.168-169

[11] F. Wu, N. Zeng, L. Zhang and D. Wu 2004 Interaction of Two-Dimensional Impulsively Started Airfoils. Journal of Marine Scienceand Application, Vol. 3, No. 1

[12] T. Sarpkaya and R. L. Shoaff 1979 Inviscid model of Two-Dimensional Vortex Shedding by a Circular Cylinder AIAA Journal, Vol. 17, No. 11, pp. 1193-1200

[13] K. Kuwahara 1978 Study of Flow past a Circular Cylinder by an Inviscid Model Journal of the Physical Society of Japan, Vol.45, No. 1, pp. 292-297

[14] A. Roy and G. Bandyopadhyay 2006 Numerical Calculation of Separated Flow Past a Circular Cylinder Using Panel Technique Journal of Wind Engineering and Industrial Aerodynamics, Vol. 94, pp-131-149

[15] J. H. Gerrard 1967 Numerical Computation of the Magnitude and Frequency of the Lift on a Circular Cylinder Phil. Trans. R. Soc. Lond., Vol. 261, pp. 137-162

[16] OpenFOAM User Guide OpenFOAM Foundation, Vol. 2, no. 1

[17] J. Katz and A. Plotkin 2001 Low-Speed Aerodynamics Cambridge University Press, Second Edition

[18] S. Ananthan and J.G. Leishman 2004 Role of filament strain in the free-vortex modeling of rotor wakes. Journal of the American Helicopter Society, Vol. 9, pp. 176-191

[19] Catalano, P., Wang, M., Iaccarino, G., Moin, P. 2003. Numerical simulation of the flow around a circular cylinder at high Reynolds numbers. International Journal of Heat and Fluid Flow, 24, 463-469

[20] Ong, M. C., Utnes, T., Holmedal, L. E., Myrhaug, D., Pettersen, B. 2009 Numerical simulation of flow around a smooth circular cylinder at very high Reynolds numbers. Marine Structures, 22(2), 142-153

[21] Bj¨ork, A. 1990A Guide to Data Files from Wind Tunnel Test of a FFA-W3-211 Airfoil at FFA. FFA-V-019, Flygtekniska F¨ors¨oksanstalten,Sweden

[22] Ramos-Garc´ıa, N., Sørensen, J.N. and Shen, W.Z. 2014 A Strong Viscous-Inviscid Interaction Model for Rotating Airfoils. Wind Energy, 17, 1957-1984. http://dx.doi.org/10.1002/we.1677

[23] Cantwell, B., Coles, D. 1983 An experimental study of entrainment and transport in the turbulent near wake of a circular cylinder. Journal of Fluid Mechanics, 136, 321-374

[24] Sarlak, H. 2014 Large Eddy Simulation of turbulent flows in wind energy. PhD Thesis, Technical University of Denmark

[25] Sarlak, H., Nishino, T. and Sørensen,J.N. 2016 URANS simulations of separated flow with stall cells over an NREL S826 airfoil. AIP Conf. Proc. 1738, 030039